Appl. Phys. A 91, 291–299 (2008)
DOI: 10.1007/s00339-008-4397-2

Applied Physics A
Materials Science & Processing

R.M.S. MARTINS[1,✉]
N. SCHELL[2]
A. MÜCKLICH[1]
H. REUTHER[1]
M. BECKERS[1]
R.J.C. SILVA[3]
L. PEREIRA[3]
F.M. BRAZ FERNANDES[3]

Study of graded Ni-Ti shape memory alloy film growth on Si(100) substrate

[1] Institute of Ion Beam Physics and Materials Research, Forschungszentrum Dresden-Rossendorf, P.O. Box 510119, 01314 Dresden, Germany
[2] Institute for Materials Research, GKSS Research Center, Max-Planck-Str. 1, 21502 Geesthacht, Germany
[3] CENIMAT, Campus da FCT/UNL, 2829-516 Monte de Caparica, Portugal

Received: 23 August 2007/Accepted: 10 December 2007
Published online: 16 February 2008 • **© Springer-Verlag 2008**

ABSTRACT In-situ X-ray diffraction (XRD) was employed to study the effect of the deliberate change of the Ti/Ni ratio during the deposition of Ni-Ti films. Thus, graded films were deposited exhibiting distinctive composition and crystalline structure along the growth direction. The as-sputtered films were ex-situ characterized by Auger electron spectroscopy (AES), cross-sectional transmission electron microscopy (XTEM), and electrical resistivity (ER) measurements (during thermal cycling). In this paper results are presented concerning a film (thickness of ≈ 420 nm) with a Ti-rich composition in the central part (ranging from 50 to ≈ 60 at. %) and near-equiatomic composition in the extremities, following four distinct deposition periods (different Ti target powers). During the initial deposition step (near-equiatomic composition) the Ni-Ti B2 phase starts by stacking onto (*h*00) planes on the naturally oxidized Si(100) substrate due to the presence of the native Si oxide (2–3 nm). The increase of the power of the Ti target in the second and third steps induced the precipitation of Ti_2Ni. When stopping the Ti co-sputtering, Ti_2Ni dissolves and, thus, plays the role of a Ti reservoir for the formation of B2 phase now preferentially stacking onto (110) with the system approaching again the equiatomic composition. The ex-situ study of the morphology of the interface has shown the presence of $NiSi_2$ silicides (A-$NiSi_2$ and B-$NiSi_2$), $Ti_4Ni_4Si_7$, Ti_2Ni and a non-identified phase constituted by Ni, Ti and Si, most likely amorphous. During thermal cycling, ER measurements revealed phase transitions associated with the B2, R-phase and B19′ phases. These type of studies allow the identification of intermediate states during deposition and annealing, and the correlation with the final structure of the film, being useful for the optimisation of the deposition parameters in order to fabricate films with a two-way reversible actuation.

PACS 81.15.Cd; 61.10.Nz; 68.55.Jk

1 Introduction

A relatively wide variety of alloys are known to exhibit the shape memory effect (SME), but only a few have received commercial exploitation. Of those, Ni-Ti alloys have been attracting keen attention due to a number of desirable properties [1, 2]. In the form of films they have also the potential for batch fabrication and, thus, Ni-Ti films are attractive materials for microfabrication and integration in micro-miniature systems composed of mechanical elements, actuators, sensors and electronics made on one chip [3–5]. They can be heated resistively, and the small thermal mass and the large surface to volume ratios allow for rapid heat transfer. Due to the high power density, and due to the large displacement and actuation force, most applications of Ni-Ti films are focused on micro-actuators, such as micropumps, microgrippers, microvalves, micropositioners, etc. [6]. Because of their sensitivity to environmental changes, e.g. thermal, and/or to stress they are also ideal materials for applications in microsensors [7]. Ni-Ti films are typically prepared using sputtering methods and though early difficulties were overcome [8–13], the deposition of Ni-Ti films with definite stoichiometry and high purity remains a challenge [14]. The precise control of the Ti/Ni ratio is essential but difficult due to the difference in sputtering yields of Ti and Ni at a given sputtering power density [15], as well as wear, erosion and roughening of targets during sputtering [16]. Several solutions were proposed to overcome this problem: adding Ti plates on the Ni-Ti target to compensate the loss of Ti [17], co-sputtering from Ni-Ti and Ti targets [16, 18] or from two separate single element (Ni and Ti) targets [19, 20], as well as varying the Ni-Ti target temperature since a heated target reduces the loss of Ti [21].

The basis of the SME is a reversible solid-state phase transformation [2]. Ni-Ti SMA transform martensitically from B2 cubic austenite into monoclinic B19′ martensite either directly or via rhombohedral R-phase [22–25]. The intermediate B2 ↔ R-phase transformation is an attractive phenomenon for actuator applications [26] because it shows a narrow hysteresis and does not vary much with cycling through the transformation range. The excellent functional fatigue properties associated with the B2 ↔ R-phase transformation, usually attributed to its small transformation strains (≈ 1%), are also a plus for these particular applications.

If the substrate is not heated during sputtering deposition, as-sputtered Ni-Ti films are amorphous [27–31], thus, a post-sputtering annealing is necessary since the thermally induced phase transformation occurs only in crystalline materials. However, films sputtered at elevated temperatures (typically above 400 °C) are crystalline as deposited. In this case,

✉ Fax: +49-351-21-294-85-58, E-mail: rmsm@fct.unl.pt

and depending on substrate type, specific fibre textures can be obtained [32, 33] and fine-grained structures are also observed [34]. Concerning the texture of Ni-Ti thin films crystallized during deposition on Si(100) substrates, Gisser et al. [35] reported that the films are highly oriented, with the B2(110) face parallel to the (100) face of the Si wafer (deposition temperature $\approx 460\,°C$). In that study, p-type Si wafers were etched with aqueous HF and rinsed with methanol before being introduced into the sputtering chamber. Liu et al. [34] observed a strong (110)-plane texture with perfect axis symmetry for a film deposited at $\approx 500\,°C$. They have used a (100) monocrystal wafer as substrate which was cleaned by "inverse" sputtering. In a previous work [36], we have shown that the Ni-Ti B2 phase starts by stacking onto (h00) planes on naturally oxidized Si(100) substrates (the native oxide layer, 2–3 nm, was not removed before deposition), and as the thickness increases evolves into a (110) fibre texture. This observation was possible using a magnetron sputtering chamber [37] especially designed to be mounted on the six-circle goniometer of the Rossendorf BeamLine (ROBL) [38] at the European Synchrotron Radiation Facility (ESRF) which allows following in-situ, the evolution of the structure of the growing film. Indeed, the ex-situ X-ray diffraction (XRD) measurements performed after deposition have shown a dominating (110) fibre texture but also the presence of a small B2(200) peak [33] as a result of the initial deposition period.

In order to further improve the properties of Ni-Ti films one considers the design of functionally graded films [6]. One possibility to achieve this goal is through the gradual change in composition (Ti/Ni ratio), crystalline structures, transformation temperatures, and/or residual stress through the film thickness. These films can be prepared by slightly changing the target powers during deposition. In this way, along the film thickness the material can exhibit different properties, e.g. changing from pseudoelasticity to SME or showing different transformation temperatures along the thickness. It is known that for Ti-rich compositions higher transformation temperatures can be achieved compared with the equiatomic or Ni-rich composition [39]. However, it is necessary to have in mind the precipitation of the Ti_2Ni phase [2, 40, 41] because a non-controlled growth of Ti_2Ni precipitates can disturb or impede the growth of martensite plates [42]. Thus, to successfully develop functionally graded Ni-Ti films it is essential to characterize, model and control the variations in composition as well as thermo-mechanical properties and the residual stress in the films [6]. In a previous publication we reported on the in-situ study of the sputter deposition of Ni-Ti SMA thin films using two targets Ni-Ti and Ti, whereby we stressed the possibilities of the real-time structural design during magnetron deposition by co-sputtering excess Ti in order to balance the mass composition and phase content of Ni-Ti films [43]. Here, a detailed structural characterization of these type of films, including the interfacial zone, and its connection with their reaction paths is reported.

2 Experimental details

Ni-Ti films were deposited by co-sputtering in a dc magnetron chamber [37]. A 25.4 mm Ni-Ti target (49 at. %Ni–51 at. %Ti) and a 25.4 mm Ti target (purity 99.99%) were inserted on the unbalanced magnetrons, which are positioned at a distance of 100 mm from the substrate surface and tilted 30° away from the substrate normal. Chimneys in front of each magnetron and the pneumatically driven blade shutters avoid cross contamination and enable sputter cleaning of the targets prior to deposition. The base pressure was approximately 2×10^{-5} Pa and the films were deposited with an Ar pressure of 0.42 Pa. The magnetron with the Ni-Ti alloy target was run at a power of 40 W while the magnetron with the pure Ti target was run at varying power levels of 0–30 W. In this series of experiments, the near-equiatomic composition could be obtained with the Ti target running at 8 W. Si(100) wafers ($15 \times 15\,mm^2$) with a natural oxide layer on top served as substrates. They were heated to a deposition and annealing temperature of $\approx 470\,°C$.

The whole deposition chamber equipped with Kapton foils as the X-ray entrance and exit windows was mounted into the six-circle goniometer of the synchrotron radiation beamline ROBL at ESRF. The radiation was monochromatized to $\lambda = 0.675$ Å (18.367 keV) and large angle XRD in Bragg–Brentano geometry was employed, thus probing the diffraction vector situated in a plane perpendicular to the plane of deposition. A sequence of scans (alternating between the scattering angles $17.0° < 2\theta < 19.5°$ and $24.3° < 2\theta < 26.8°$) were performed, each one taking approximately 2 min, in order to monitor the XRD peaks of the Ni-Ti B2(110) and B2(200); these scans are intended to reveal the type of preferential orientation during the deposition process and to determine off-plane lattice parameters variations. After deposition and naturally cooling to room temperature (RT) the samples were quenched into liquid nitrogen and then let warm up to RT.

Atomic depth profiles were determined by Auger electron spectroscopy (AES) with a scanning Auger electron spectrometer Microlab 310F (Fisons Instruments). Cross-sectional transmission electron microscopy (XTEM) observations were carried out on a Philips CM300 microscope with a LaB_6 filament at 300 keV (without intentional heating of the sample). For this purpose, the samples were prepared by gluing two pieces film to film and then cutting a perpendicular section, which was thinned by mechanical grinding. Final thinning to electron transparency was accomplished using 5 keV Ar^+ ion milling.

A four-probe experimental apparatus (van der Pauw geometry) was used to measure the electrical resistivity (ER) of the films as a function of temperature in order to investigate phase transformations. The thermal cycles comprised

(i) heating from RT up to 110 °C, followed by
(ii) cooling down to −110 °C, and finishing by
(iii) heating up to 110 °C again.

The analysis of the transformation behaviour was based on the cycles (ii) and (iii). The measurements were performed with the Ni-Ti films attached to the substrate.

3 Results

3.1 *In-situ XRD characterization*

Figure 1 demonstrates the benefit of following in-situ the evolution of the structure of the film (during growth,

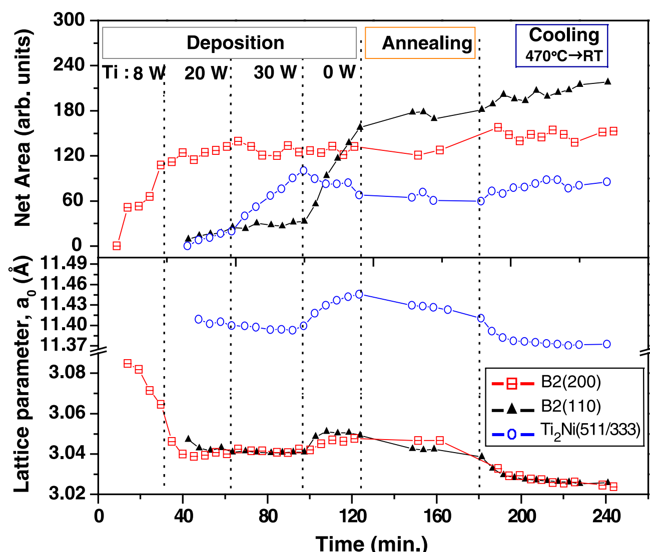

FIGURE 1 In-situ XRD results for a Ni-Ti graded film deposited on naturally oxidized Si(100) during continuous co-sputtering of Ni-Ti (40 W) and Ti (8/20/30/0 W), and during annealing. Represented are the integrated intensities of the Bragg–Brentano B2(110), B2(200) and $Ti_2Ni(333/511)$ diffraction peaks as well as the lattice parameters as obtained from the positions of the respective Bragg–Brentano peaks, as a function of time

annealing and cooling from deposition to RT), revealing intermediate conditions, which cannot be observed by ex-situ techniques. In this experiment the magnetron with the Ni-Ti alloy target was run at a constant power of 40 W during the four steps of the deposition while the magnetron with the pure Ti target was run at 8, 20 and 30 W on the 1st, 2nd and 3rd deposition steps, respectively. The chosen sequence and amount of co-sputtering led to different peak intensities of the various phases. In the figure are represented the variation of the integrated intensities of B2 and Ti_2Ni peaks (B2(110), B2(200) and $Ti_2Ni(333/511)$, respectively) and the variation of the lattice parameter a_0 (as calculated from d according to the corresponding Bragg–Brentano peak position), as a function of time after start of deposition. Under the chosen deposition parameters the B2 phase starts by stacking onto (h00) planes. During this initial period of the deposition a significant change of the lattice parameter as calculated from $d_{(200)}$ is observed. This is a typical behaviour already observed by our group during the deposition of near-equiatomic films on naturally oxidized Si(100) substrates [36]. In that previous study, after the formation of a strained layer with the B2 phase with (h00) planes parallel to the substrate during the first 30 min, it relaxed, and then the diffracted intensity of B2(200) stayed constant while the B2(110) intensity was linearly growing. Here, after this initial period (≈ 30 min), the Ti co-sputtering power was increased to 20 W and, consequently, the $Ti_2Ni(333/511)$ peak together with the B2(110) peak were detected. A further increase of co-sputtered Ti in the film (increasing the Ti magnetron power to 30 W) enhances the development of the Ti-rich phase. During co-sputtering with a Ti power of 30 W the lattice parameter values of B2 phase as calculated from $d_{(200)}$ and $d_{(110)}$ are already quite stable, while for Ti_2Ni, as calculated from $d_{(333/511)}$, a continuous slight decrease of this value is perceptible. After approximately 97 min by stopping the Ti co-sputtering (i.e. increasing the Ni/Ti ratio of the atoms deposited at the growing film), Ti_2Ni dissolves and, thus, plays the role of a Ti reservoir for the formation of B2 phase now preferentially stacking onto (110). A significant increase of a_0 value of the Ti_2Ni as calculated from $d_{(333/511)}$ is observed. For B2 phase the increase is slightly higher for the value calculated from $d_{(110)}$. During the annealing step no relevant peak intensity changes, i.e. no structural or phase changes, could be discerned. However, just the a_0 value of B2 as calculated from $d_{(200)}$ stays stable. The a_0 value of B2 as calculated from $d_{(110)}$ and the one calculated for Ti_2Ni decrease. The cooling stage from deposition temperature to RT results in an overall decrease of a_0 for both phases, and for the B2 phase the values calculated from $d_{(110)}$ and $d_{(200)}$ are comparable.

3.2 *Ex-situ AES and XTEM characterization of the structural depth profile*

The depth profile of the atomic concentrations in the Ni-Ti film from Fig. 1 is shown in Fig. 2. For the AES and XTEM results presented, the substrate can be found on the right hand side. In Fig. 2 the different steps of co-sputtering deposition are marked with dashed lines and identified by Roman numerals. The manipulation of the Ti power resulted in a non-homogeneous composition along the cross-section of the film, and the first fraction of the film (I), supposed to exhibit a near-equiatomic composition, shows evidence of an interfacial reaction between the film and the substrate as deduced from the altered composition nearby the substrate. Starting the evaluation from the interface to the surface of the film, Ni and Ti are detected in the Si substrate. Ni atoms appear to be the primary diffusing species into the substrate. There is also considerable inter-diffusion of Si atoms into the Ni-Ti film, therefore, a near-equiatomic composition in fraction I is only obtained at a distance from the interface where diffusion is no longer relevant. Fraction II is richer in Ti and proportionally poorer in Ni due to the increase of the Ti power to 20 W. The consequence of the additional increase to 30 W is also clearly perceptible in fraction III but

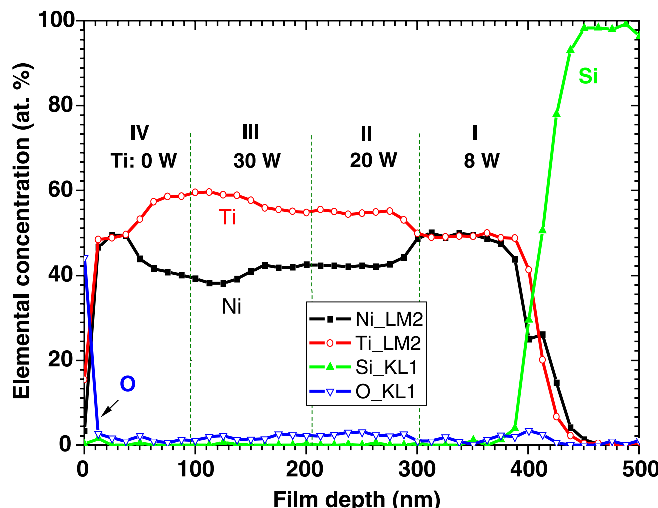

FIGURE 2 AES elemental concentration profiles for the Ni-Ti sample from Fig. 1 (graded film)

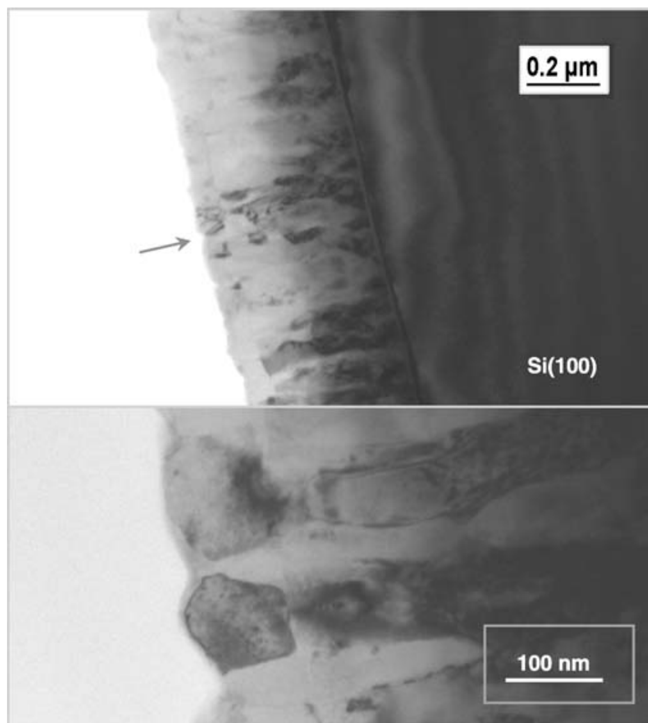

FIGURE 3 XTEM micrograph from the Ni-Ti graded film on the naturally oxidized Si substrate recorded along the Si[110] zone axis, with an enlargement of the topmost film's region

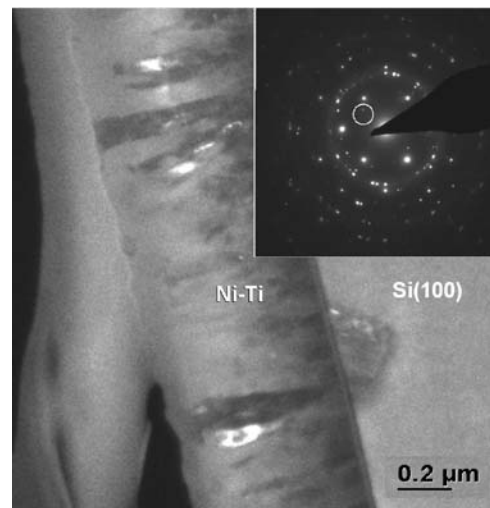

FIGURE 4 SAED pattern obtained on the overall cross-section of the Ni-Ti graded film, with a delimitation of the spot associated with Ti_2Ni(220), and the XTEM dark field image resulting from the selection of this spot. The respective Ti_2Ni precipitates show up as bright regions in the XTEM micrograph

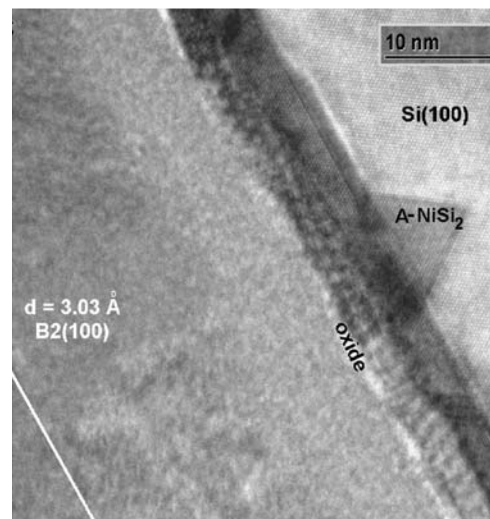

FIGURE 5 XTEM micrograph showing the structure of the graded film near the interface. The B2(100) planes parallel to the interface were identified as well as the presence of distinct phases in the reaction product at the interface

the most interesting is the tendency of the system to achieve the near-equiatomic composition during the last deposition step (fraction IV). Most likely, the observed composition variation in fraction IV is mainly the result of stopping the Ti co-sputtering and consequently a Ti_2Ni dissolution. During the annealing period no relevant intensity changes could be discerned by in-situ XRD.

Figure 3 shows a XTEM micrograph from the Ni-Ti film on the Si substrate recorded along the Si[110] zone axis, with an enlargement of the topmost region of the film (indicated with the arrow). Apart from the columnar structure, a topmost layer with different contrast (apparently showing also different morphology) is clearly visible. This altered fraction of the film is a result of the last deposition step, i.e. only with the Ni-Ti target running there is a dissolution of the Ti_2Ni rich precipitates formed in the preceding two steps (see fraction IV of Fig. 2).

A selected-area electron diffraction (SAED) pattern obtained on the overall cross-section of the Ni-Ti film is presented in the inset of Fig. 4. By choosing the spot delimited in the SAED pattern, which is associated with Ti_2Ni(220), the respective precipitates show up as bright regions in the corresponding XTEM dark field image of Fig. 4. They are generally detected in the central zone being in agreement with the depth profile of Fig. 2. The Ti content exceeds largely the one of Ni in this zone (fractions II and III).

The XTEM micrograph of Fig. 5 shows the structure of the film nearby the interface. The B2(100) planes parallel to the interface were identified by high-resolution (HR)-XTEM (fast Fourier transformation procedure). By in-situ XRD (Fig. 1) it was observed that the B2 phase starts by stacking onto (h00) planes which is in conformity with XTEM observations. It also suggests that the film near the interface (fraction I in Fig. 2) is austenitic at RT. Figure 5 also gives evidence of the presence of distinct phases in the reaction product at the interface. Between the Ni-Ti B2 structure (with the (100) planes parallel to the interface) and the oxide layer (most probably a (Si, O)-rich layer, i.e. the native silicon oxide of the Si substrate), a lighter grey layer can be distinguished. This phase could not be identified by HR-XTEM, suggesting that no crystalline order is present. The same was observed for other samples with this type of interfacial morphology (near-equiatomic Ni-Ti films on naturally oxidized Si(100) substrates). On the substrate side, $NiSi_2$ forms epitaxially towards the Si substrate, which agrees with the finding of Ni deeper inside the substrate in Fig. 2. A detailed analysis of the interfacial structure can be found in the next section.

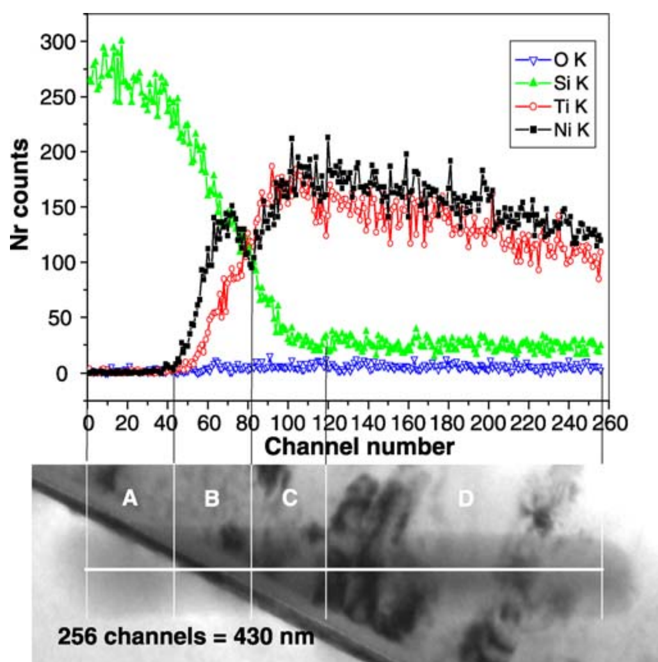

FIGURE 6 EDS results obtained using the line scan mode of the transmission electron microscope along a distance of 430 nm, probing information from the substrate, interface and the Ni-Ti graded film

3.3 *Ex-situ XTEM characterization of the interfacial structure*

The EDS system of the transmission electron microscope (electron dispersive X-ray spectroscopy technique) was used in order to identify the elements present in the different reaction layers. Figure 6 shows the results obtained using the line scan mode along a distance of 430 nm, probing information from the substrate, interface and Ni-Ti film. With this complementary information provided by the EDS measurement it is possible to conclude that the lighter grey layer located between the Ni-Ti B2 structure and the Si oxide layer has in its composition not only Ni and Ti but also Si (see part C in Fig. 6). This confirms the diffusion of Si into the alloy and suggests the presence of ternary silicides. An expected increase of the Ni content in the interface substrate's side (part B) is discernible mainly as a result of the formation of $NiSi_2$ compounds (detected in Fig. 5).

The XTEM micrographs of the morphology of the interface presented in Fig. 7 were obtained on a different sample, deposited with constant deposition parameters, which resulted in a near-equiatomic composition (all the other results in the paper were obtained for the graded film). However, the interface morphology is analogous and since for this sample higher quality images could be achieved, we show here the respective micrographs in order to provide more information about the reaction phases. The main micrograph in Fig. 7 clearly shows that A-$NiSi_2$ silicides grow epitaxially towards the Si substrate with growth fronts {111} resulting in a semi-octahedron shape. A deeper insight into the circled area can be found in the inset of the figure. In the Si oxide layer of the substrate it is possible to distinguish the presence of disruptions. The $Ti_4Ni_4Si_7$ compound (identified by HR-XTEM) nucleates between the oxide layer and the A-$NiSi_2$. However,

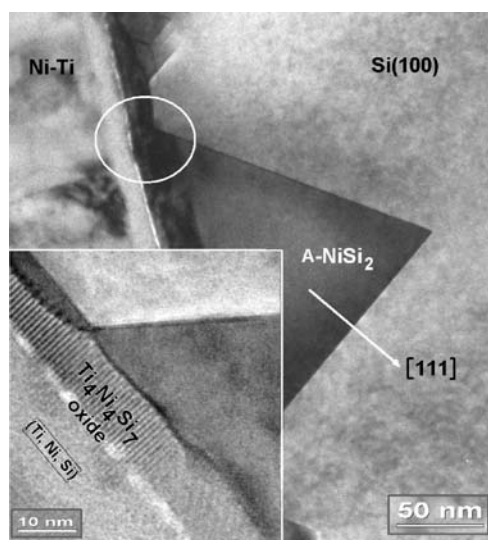

FIGURE 7 XTEM micrographs of the interface's morphology obtained on a sample, deposited with constant deposition parameters, which resulted in a near-equiatomic composition. The *main micrograph* shows that A-$NiSi_2$ silicide grows epitaxially towards the Si substrate with growth fronts [111] resulting in a semi-octahedron shape. The *inset* represents the *circled region* in high resolution

the compound (with Ni, Ti and Si in its composition), which forms between the oxide layer and the Ni-Ti film, could not be identified as already mentioned (lighter grey layer).

In Fig. 8 the interfacial reaction products of the graded film are not all visible because the focus was in the area on the left hand side of the lighter grey layer (region of the film). A dashed line is inserted on top of the thin oxide layer as a reference. The goal has been the detection of possible Ti_2Ni phase. Stemmer et al. [44] mention the formation of a Ti-rich layer with no significant amount of silicon that was associated with the Ti_2Ni compound. This layer adjacent to the Ni-Ti near-equiatomic film could be the result of the migration of

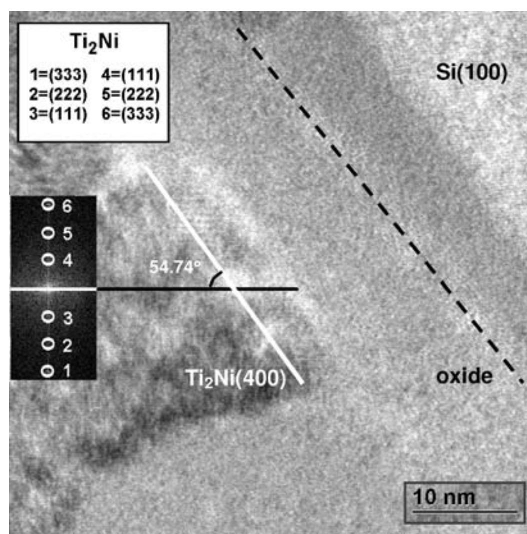

FIGURE 8 XTEM micrograph of the interfacial zone of the graded film with a *black line* inserted on top of the thin oxide layer as a reference. Lattice spacings agreeing well with those of Ti_2Ni were observed suggesting that the (111) planes of Ti_2Ni make with the interface an angle that leads the (400) planes approximately parallel to the interface

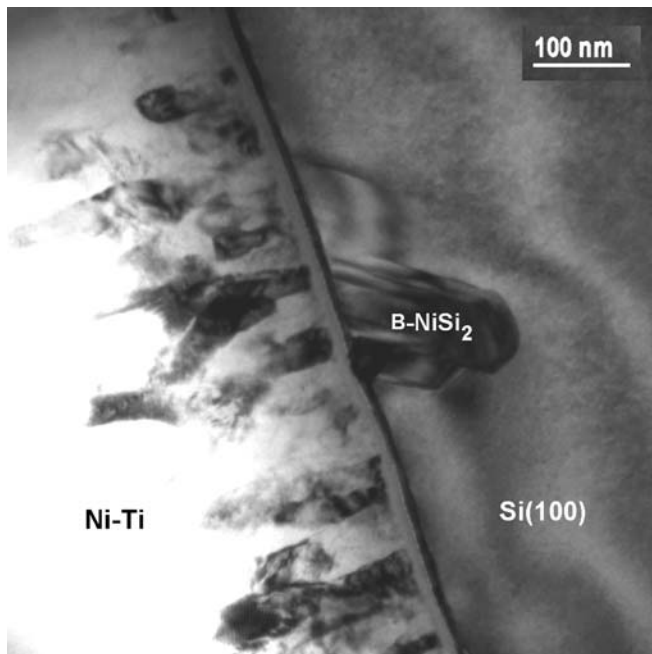

FIGURE 9 XTEM micrograph (graded Ni-Ti film) focusing the presence of the B-$NiSi_2$ in the Si(100) substrate

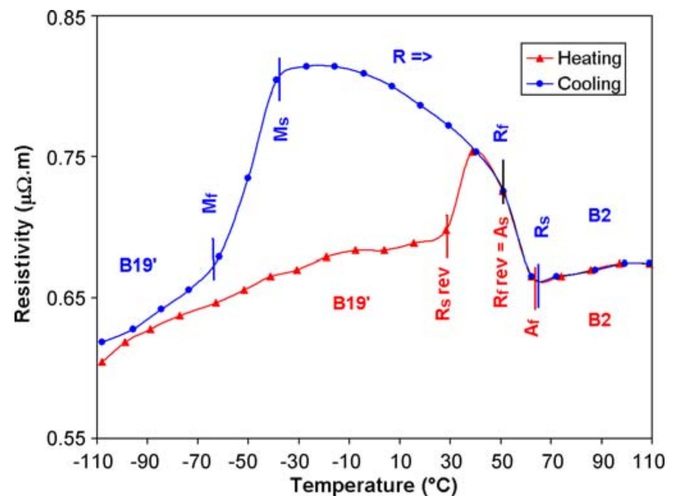

FIGURE 10 Dependence of electrical resistivity in the Ni-Ti graded film with temperature during cooling and heating

the Ni atoms, which are the main species diffusing at the TiNi-Si interface below 600 °C [45]. In our study, in some areas along the interface, lattice spacings agreeing well with those of Ti_2Ni were observed between the Ni-Ti film and the lighter grey layer (ternary compound: Ti, Ni, Si). The (111) planes of Ti_2Ni were identified making an angle with the interface that leads to the (400) planes being approximately parallel to the interface. A line on the figure indicates the expected arrangement of the (400) planes.

It should be pointed out that there are two possible $NiSi_2$ families:

(i) A-precipitates, which grow epitaxially to the Si host lattice with growth fronts {111} resulting in a semi-octahedron shape (see Figs. 5 and 7),
(ii) B-precipitates, with a twin orientation (rotation by 180° around the [111]).

In this work, the formation of B-$NiSi_2$ precipitates in the Si substrate was also detected (Fig. 9).

3.4 *Study of the transformation temperatures*

The ER versus temperature response of the graded Ni-Ti film during thermal cycling is shown in Fig. 10. In the graph, R_s, R_f, M_s, M_f and A_s, A_f are the temperatures for the start and finish of the formation of the intermediate R-phase and B19′, on cooling, and B2, on heating. The resistivity value decreases linearly with the temperature during cooling from 110 °C down to R_s. Self-accommodation R-phase transformation starts at R_s and the austenite parent phase (B2) begins to transform to the twinned R-phase with further decrease of the temperature. Twinning in an alloy matrix results in electron scattering that in turn leads to the increase of the ER [46]. The twinned structure density in B2 phase increases with the decrease of the temperature (due to the B2 → R-phase transformation), producing a higher ER as a result of the more pronounced increase of lattice imperfections compared to the decrease of the resistance due to electron scattering by phonons. R-phase transformation ends once the temperature decreases to R_f. An additional cooling promotes the R-phase distortion (R ⇒) and at M_s the R-phase starts transforming to monoclinic B19′ martensite, which exhibits less lattice distortion. The martensite transformation finishes when the temperature decreases to M_f and cooling below M_f does not result in more phase changes.

On heating, the R-phase reverse transformation leads to a rapid increase in the ER and we suggest that the film completely transforms to R-phase before transforming to B2 (that's why the local maximum is there). The R_f reverse temperature is not put at the maximum point because two processes overlap upon heating: (i) B19′ → R-phase and (ii) R ⇐ (decreasing distortion). The transformation from R-phase to cubic B2 austenite parent phase leads to detwinning and rapid decrease in the ER. It is completed at temperature A_f and the microstructure completely reverses to the original microstructure consisting of single cubic B2 austenite.

4 Discussion

The in-situ XRD measurements have shown that for a near-equiatomic composition the Ni-Ti B2 phase starts by stacking onto (h00) planes on a naturally oxidized Si(100) substrate (Fig. 1). We attribute to the native Si oxide a key role for this preferential stacking. Kim et al. [32] proposed that a strong interfacial adsorption on the heated substrate promotes the preferential coverage by a first layer of Ti on top of thermally oxidized Si substrates. This leads to the preferential formation of the (h00)-oriented Ni-Ti film since, in the B2 cubic structure, the (h00) planes are alternately occupied by Ni and Ti atoms. In an earlier work [36] we have confirmed the role of the oxide layer on the development of the (100) orientation of the B2 phase during the deposition on heated substrates (≈ 470 °C). Gisser et al. in [35] where they reported that Ni-Ti films crystallized during the deposition process are highly oriented, with the B2(110) face parallel to the (100)

face of the Si wafer, mentioned peak intensity ratios for the B2 phase ((110), (200) and (211) peaks) of 50 000 : 1 : < 1. The B2(200) peak does not quite disappear, but was too small to be seen without rescaling the data. In contrast, when we deposited near-equiatomic films on naturally Si(100) substrates the B2(200), which appears at the beginning of the deposition, can be detected without rescaling the data as can be observed in [33]. The reason for this difference is most likely the fact that they have used Si wafers etched with aqueous HF and rinsed with methanol and in our case the native Si oxide layer (2–3 nm) was not removed before Ni-Ti deposition.

Considering the evolution of the lattice parameter a_0 as calculated from $d_{(200)}$ during the initial deposition stage, a considerable reduction of compressive stresses with increasing thickness is observed. Probably the higher variation of the stress state in the beginning of the deposition, i.e. next to the interface film/substrate, is also related to the interfacial reactions processes [47, 48]. Gisser et al. [35] also observed in their samples that the film stress parallel to the substrate is compressive (by ex-situ measurements). Having the Si substrate peak as an internal standard, they obtained larger d-spacings for the B2(110) when compared with the same plane in bulk Ni-Ti. Furthermore, Grummon and Zhang [49] have observed a variation of the intrinsic stress with film thickness. A decrease of the compressive stress from −430 MPa for 1.3 μm thick films to −250 MPa for 4.2 μm thick material was reported. A dependence was suggested between the intrinsic stress developed and the effective shear compliance of the substrate, such that for the initial deposited layers the Ni-Ti film experiences a substrate compliance identical to that of pure Si(100), developing large compressive stresses.

In our previous experiments, during the study of the growth of near-equiatomic Ni-Ti films (2 h deposition) [36], with increasing film thickness a crossover of the crystallographic orientation into a (110) preferred orientation is observed (≈ 30 min after deposition start), which is the more densely packed crystallographic plane [50]. The preferential stacking of B2 phase on (110) planes is coincident with the deposition time where a tendency for the stabilization of the lattice parameter as calculated from $d_{(200)}$ is detected (significantly decrease of compressive stress). However, in the present work, after this initial deposition period of ≈ 30 min, the Ti co-sputtering power was increased, first to 20 W and later to 30 W, leading to the desired precipitation of the Ti-rich phase Ti_2Ni. During the precipitation process the lattice parameter value of Ti_2Ni, as calculated from $d_{(333/511)}$, slight decreases in a continuous way. Ishida et al. [51] observed that when an amorphous Ti-rich Ni-Ti thin film is crystallized (Ti-48.2 at. %Ni in the study), the microstructure changes in the sequence of

(1) Guinier–Preston (GP) zones,
(2) GP zones and Ti_2Ni precipitates within Ni-Ti grains,
(3) Ti_2Ni precipitates within Ni-Ti grains, and
(4) Ti_2Ni precipitates along grain boundaries.

The microstructure of a sample annealed at 500 °C for 1 h was reported to have a dispersion of Ti_2Ni inside the Ni-Ti grains, as well as GP zones. The Ti_2Ni has partial coherency with the matrix and the misfit is considerably relaxed. They found the close relationship between the Ti_2Ni precipitates and the Ni-Ti matrix, and observed some similarity between the units cells of both phases. A high magnification image of the interface in their study revealed that some of the {110} planes are continuous through the precipitate and the matrix. Since the lattice parameter of Ti_2Ni and the one of Ni-Ti exhibit a difference slightly less than four times, if the Ti_2Ni precipitate is coherent with the matrix at the beginning of the precipitation process, a stress field is formed around the precipitate. In the present paper, we cannot directly compare the results with that obtained by Ishida et al. [51], because here the Ni-Ti film is crystallized during the deposition process. Nevertheless, we should consider that the continuous slight decrease of the lattice parameter value of Ti_2Ni, as calculated from $d_{(333/511)}$, could also be associated with the formation of a stress field around the precipitate.

During the last deposition period (without Ti co-sputtering), Ti_2Ni dissolves and, thus, plays the role of a reservoir for the formation of B2 phase now preferentially stacking onto (110). As suggested by the depth profile results of the atomic concentrations (Fig. 2) this dissolution process is a consequence of the shift of the global composition towards Ni-richer, ending up at the near-equiatomic composition. Since no relevant peak intensity changes could be discerned by in-situ XRD during the annealing period, the main progress to reach the near-equiatomic composition occurs certainly during this last deposition step. During this step a significant increase of the a_0 value of the Ti_2Ni is observed and for the B2 phase the increase is slightly higher for the value calculated from $d_{(110)}$. The variation observed for the a_0 value of the B2 phase can be related to the incorporation of Ti in the matrix. We should also consider that if this dissolution process leads to the formation of GP zones, compressive stress fields in the matrix around them will be produced.

A detailed analysis of the morphology of the interface Ni-Ti/naturally oxidized Si(100) was performed resulting in the identification of several phases. $NiSi_2$ silicides (A-$NiSi_2$ and B-$NiSi_2$) were detected on the substrate's side as well as $Ti_4Ni_4Si_7$. A different ternary silicide type (not identified) and Ti_2Ni is perceptible on the Ni-Ti film's side (Fig. 7, 8 and 9). The native silicon oxide layer of the Si substrate is used here as a reference in this delimitation (substrate's side and film's side). For the deposition of near-equiatomic Ni-Ti films on naturally oxidized Si(100) at high temperature (≈ 470 °C) Ni atoms migrate from the Ni-Ti film to the Si substrate leading to disilicide formation. Wu et al. [45] reported that the development of $NiSi_2$ instead of NiSi or Ni_2Si might be due to the (Si, O)-rich layer (native silicon oxide layer), which reacts against the diffusion of Ni atoms, resulting in a lower Ni supply rate. Using a Ni/Ti bilayer system on Si(100) substrates, Falke et al. [52] also found a preferential growth of epitaxial $NiSi_2$ at reaction temperatures of about 475 °C, i.e., the nickel disilicide phase forms first. This was associated with the relatively slow Ni transport rate through the Ti layer, which acts as a diffusion rate-limiting barrier.

The migration of Ni from the Ni-Ti film leaves the film adjacent to the interface depleted in Ni and the Ti-rich Ti_2Ni phase is formed having been detected in some areas along the interface in our study (in this zone of the film the appearance of Ti_2Ni phase is not related to the increase of the power of the Ti target). The (111) planes of Ti_2Ni were iden-

tified making an angle with the interface that leads to the (400) planes approximately parallel to the interface. In the areas where the Ti_2Ni is present, the B2 phase was identified and the (100) planes are parallel to the interface. Published studies concerning the crystallization of Ti-rich Ni-Ti films at temperatures above crystallization temperature report granular Ti_2Ni precipitates [2]. In this temperature regime two situations with respect to the orientation relationship to the B2 matrix were identified. For a Ti content lower than 53%, Ti_2Ni precipitates have a specific orientation relationship to the matrix (B2 phase), because the precipitates are formed after the crystallization of the B2 matrix. In this case it is expected that the crystal axes of Ti_2Ni and those of B2 are parallel to each other. On the contrary, when the Ti content is higher, the Ti_2Ni phase is formed first, and then crystallization occurs and no orientation relationship between the precipitate and matrix could be identified. Based on the information provided by these earlier studies, we believe that it is not a coincidence to find Ti_2Ni with (400) planes approximately parallel to the interface in the B2 matrix with the (100) planes parallel to the interface. It seems that after the deposition and crystallization of a near-equiatomic film fraction, the diffusion process led to the formation of Ti_2Ni precipitates apparently with an orientation relationship with the matrix.

The Si and Ti atoms also migrate probably at a lower rate than Ni since the formation of nickel silicide is less sensitive to the O-rich layer than the formation of titanium silicide in the Ti/Si-substrate system [53]. A near-$Ti_4Ni_4Si_7$ compound nucleates at the interface and, for higher temperatures, according to the results from Wu et al. [45] it would grow into the A-$NiSi_2$ and the Si substrate. A ternary compound (Ti, Ni, Si) of a different type also nucleates at the interface and grows into the Ni-Ti film. Wu et al. [45] observed a ternary silicide in this region and mentioned that it has a stoichiometry close to TiNiSi. However, in our case this phase could not be identified by HR-XTEM, suggesting that no crystalline order is present.

The deposition of Ni-Ti graded films and respective in-situ and ex-situ characterization allowed us not only to obtain essential information concerning the structural development of Ni-Ti films on naturally oxidized Si(100) substrates but also the production of Ni-Ti films exhibiting phase transformations was achieved. The temperature dependence results of the ER presented in Fig. 10 for cooling and heating show the phase transformation behaviour of the graded film. During thermal cycling B2, R-phase and B19′ phases are detected. It is usually mentioned that the intermediate transformation to the rhombohedral R-phase can be observed if the Ni-Ti alloy is subject to specific processing conditions like: variation of Ni content, introduction of a ternary element, thermal annealing, thermal cycling or cold working [24]. However, the R-phase transformation has been already observed in Ti-rich Ni-Ti thin films fabricated by sputtering, possessing Ti_2Ni precipitates with a specific orientation relationship with the Ni-Ti matrix and strong strain fields around them [51]. Nam et al. [54] also reported for Ti-rich Ni-Ti alloy ribbons made by melt spinning the presence of Ti_2Ni particles with an orientation relationship to the B2 phase and coherency strains around them, which was thought to play an important role to induce the R-phase transformation. In view of these results, we suggest also for our samples a link between the Ti_2Ni precipitates and the R-phase transformation.

The temperature dependence results of the ER raise another important question. By the transformation temperatures, the existence of B2 phase at RT is not expected but HR-XTEM images have shown lattice spacings agreeing well with those of B2 phase near the interface film/substrate (see Fig. 5). These images were obtained without intentional heating of the TEM sample holder but it is necessary to take into consideration that the electron microscope *e*-beam can provide energy and consequently heating of the film. In case the phase transformation temperature of this area of the film is only a few degrees above RT, the *e*-beam can possibly provide enough energy to cause the phase transformation. Johnson et al. [55] demonstrated the actuation of a micro-scale device by using electron-beam (ISI60 scanning electron microscope) heating. Nevertheless, we believe that this is not the reason for the detection of the B2 phase near the interface in our measurements. Su et al. [56] observed (by XTEM) for films deposited on thermally Si oxidized substrates (200 nm SiO_2 layer) an interlayer adjacent to the substrate which never transforms to martensite even though the above layer shows a clear transformation microstructure, presumably due to the mechanical constraints imposed by the substrate. The untransformed interlayer, consisting of parent phase and about 50–100 nm thick, has been found in films of various thicknesses. Fu et al. [57] studied the effects of film thickness on phase transformation of constrained $Ni_{49.8}Ti_{50.2}$ films deposited onto Si(100) substrates (the Si wafers were ultrasonically cleaned in acetone, methanol and then de-ionised water, successively). They have found a minimum thickness (about 100 nm for the Ni-Ti film) necessary to guarantee apparent phase transformation behaviours in the films. For very thin films the surface oxide and interfacial diffusion layers exert a dominant constrained effect that renders high residual stress and low recovery stress in the film. The detection of the B2 phase near the interface film/substrate in our study is in agreement with those two works.

5 Summary

The growth of Ni-Ti graded films on naturally oxidized Si(100) substrates was investigated by in-situ XRD complemented with ex-situ analysis techniques. During co-sputtering deposition the Ti/Ni ratio was deliberately changed by varying the power of the Ti target, thus depositing films with distinctive composition and crystalline structure across the film thickness. For a near-equiatomic composition the Ni-Ti B2 phase starts by stacking onto (*h*00) planes and the in-situ XRD measurements suggest that the film experiences compressive stresses, which are significantly relaxed with increasing thickness. A detailed analysis of the morphology of the interface revealed the presence of $NiSi_2$ silicides (A-$NiSi_2$ and B-$NiSi_2$), $Ti_4Ni_4Si_7$, Ti_2Ni as well as a non-identified amorphous phase constituted by Ni, Ti and Si. The temperature dependence results of the ER for cooling and heating have detected variations of the resistivity values associated with the B2, R-phase and B19′ phases transitions. This work allowed the identification of different phenomena on the growth of graded Ni-Ti films on naturally oxidized Si(100), thus leading

to the optimisation of the deposition parameters for future fabrication of films with a combination of pseudoelasticity and shape memory characteristics.

ACKNOWLEDGEMENTS The authors would like to thank the FCT/MCTES for a Ph.D. scholarship (POCI 2010/FSE for R.M.S.M.), U. Strauch and Márcia Silva for the support of the experiments at ROBL, and the DAAD (German Academic Exchange Service) for financial support under contract D/05/50641 within the program Acções Integradas Luso-Alem as/DAAD-Grices 2006. Thanks are also due to P. Šittner and V. Novák from the Academy of Sciences of the Czech Republic for fruitful discussions and to Professor E. Fortunato for the use of the fourprobe apparatus for the electrical resistivity measurements at CENIMAT. The financial support from ESRF for experiments at ROBL as well as the pluriannual financial support of CENIMAT from FCT/MCTES are gratefully acknowledged by R.J.C.S., L.P. and F.M.B.F.

REFERENCES

1 K. Otsuka, T. Kakeshita, MRS Bull. **27**, 91 (2002)
2 K. Otsuka, X. Ren, Prog. Mater. Sci. **50**, 511 (2005)
3 R.H. Wolf, A.H. Heuer, J. Microelectromech. Syst. **4**, 206 (1995)
4 P. Krulevitch, A.P. Lee, P.B. Ramsey, J.C. Trevino, J. Hamilton, M.A. Northrup, J. Microelectromech. Syst. **5**, 270 (1996)
5 H. Kahn, M.A. Huff, A.H. Heuer, J. Micromech. Microeng. **8**, 213 (1998)
6 Y. Fu, H. Du, W. Huang, S. Zhang, M. Hu, Sens. Actuators A **112**, 395 (2004)
7 M. Bendahan, K. Aguir, J.L. Seguin, H. Carchano, Sens. Actuators **74**, 242 (1999)
8 J.A. Walker, K.J. Gabriel, M. Mehregany, Sens. Actuators A **21**–**23**, 243 (1990)
9 J.D. Busch, A.D. Johnson, C.H. Lee, D.A. Stevenson, J. Appl. Phys. **68**, 6224 (1990)
10 A.P. Jardine, H. Zhang, L.D. Wasielesky, Mater. Res. Soc. Symp. Proc. **187**, 181 (1990)
11 J.D. Johnson, J. Micromech. Microeng. **1**, 34 (1991)
12 A.P. Jardine, J. Vac. Sci. Technol. A **13**, 1058 (1995)
13 A. Ishida, V. Martynov, MRS Bull. **27**, 111 (2002)
14 B. Winzek, S. Schmitz, H. Rumpf, T. Sterzl, R. Hassdorf, S. Thienhaus, J. Feydt, M. Moske, E. Quandt, Mater. Sci. Eng. A **378**, 40 (2004)
15 K.K. Ho, K.P. Mohanchandra, G.P. Carman, Thin Solid Films **413**, 1 (2002)
16 C.-L. Shih, B.-K. Lai, H. Kahn, S.M. Phillips, A.H. Heuer, J. Microelectromech. Syst. **10**, 69 (2001)
17 S. Miyazaki, A. Ishida, Mater. Sci. Eng. A **273**–**275**, 106 (1999)
18 R.M.S. Martins, N. Schell, R.J.C. Silva, L. Pereira, K.K. Mahesh, F.M.B. Fernandes, Sens. Actuators B **126**, 332 (2007)
19 A. Ohta, S. Bhansali, I. Kishimoto, A. Umeda, Sens. Actuators A **86**, 165 (2000)
20 S. Sanjabi, Y.Z. Cao, S.K. Sadrnezhaad, Z.H. Barber, J. Vac. Sci. Technol. A **23**, 1425 (2005)
21 K.K. Ho, G.P. Carman, Thin Solid Films **370**, 18 (2000)
22 D. Shindo, Y. Murakami, T. Ohba, MRS Bull. **27**, 121 (2002)
23 H. Sitepu, W.W. Schmahl, D.M. Toebbens, Textures Microstruct. **35**, 185 (2003)
24 T. Goryczka, H. Morawiec, J. Alloys Compd. **367**, 137 (2004)
25 J. Khalil-Allafi, W.W. Schmahl, D.M. Toebbens, Acta Mater. **54**, 3171 (2006)
26 P. Šittner, M. Landa, P. Lukáš, V. Novák, Mech. Mater. **38**, 475 (2006)
27 J.-M. Ting, P. Chen, J. Vac. Sci. Technol. A **19**, 2382 (2001)
28 J.Z. Chen, S.K. Wu, J. Non-Cryst. Solids **288**, 159 (2001)
29 H.-J. Lee, H. Ni, D.T. Wu, A.G. Ramirez, Appl. Phys. Lett. **87**, 114 102-1 (2005)
30 H.-J. Lee, H. Ni, D.T. Wu, A.G. Ramirez, Appl. Phys. Lett. **87**, 124 102 (2005)
31 R.M.S. Martins, F.M.B. Fernandes, R.J.C. Silva, L. Pereira, P.R. Gordo, M.J.P. Maneira, M. Beckers, A. Mücklich, N. Schell, Appl. Phys. A **83**, 139 (2006)
32 I.-J. Kim, H. Nanjo, T. Iijima, T. Abe, Japan. J. Appl. Phys. **39**, 568 (2000)
33 R.M.S. Martins, N. Schell, M. Beckers, R.J.C. Silva, K.K. Mahesh, F.M.B. Fernandes, Mater. Sci. Eng. A, DOI:10.1016/j.msea.2006.12.225 (2007)
34 Y.S. Liu, D. Xu, B.H. Jiang, Z.Y. Yuan, P. van Houtte, J. Micromech. Microeng. **15**, 575 (2005)
35 K.R.C. Gisser, J.D. Busch, A.D. Johnson, A.B. Ellis, Appl. Phys. Lett. **61**, 1632 (1992)
36 R.M.S. Martins, N. Schell, M. Beckers, K.K. Mahesh, R.J.C. Silva, F.M.B. Fernandes, Appl. Phys. A **84**, 285 (2006)
37 W. Matz, N. Schell, W. Neumann, J. Bøttiger, J. Chevallier, Rev. Sci. Instrum. **72**, 3344 (2001)
38 W. Matz, N. Schell, G. Bernhard, F. Prokert, T. Reich, J. Claußner, W. Oehme, R. Schlenk, S. Dienel, H. Funke, F. Eichhorn, M. Betzl, D. Pröhl, U. Strauch, G. Hüttig, H. Krug, W. Neumann, V. Brendler, P. Reichel, M.A. Denecke, H. Nitsche, J. Synchroton Radiat. **6**, 1076 (1999)
39 P. Surbled, C. Clerc, B.L. Pioufle, M. Ataka, H. Fujita, Thin Solid Films **401**, 52 (2001)
40 A.S. Paula, J.H.P.G. Canejo, K.K. Mahesh, R.J.C. Silva, F.M.B. Fernandes, R.M.S. Martins, A.M.A. Cardoso, N. Schell, Nucl. Instrum. Methods B **246**, 206 (2006)
41 M.J. Vestel, D.S. Grummon, Mater. Sci. Eng. A **378**, 437 (2004)
42 J.X. Zhang, M. Sato, A. Ishida, Acta Mater. **51**, 3121 (2003)
43 N. Schell, R.M.S. Martins, F.M.B. Fernandes, Appl. Phys. A **81**, 1441 (2005)
44 S. Stemmer, G. Duscher, C. Scheu, A.H. Heuer, M. Rühle, J. Mater. Res. **12**, 1734 (1997)
45 S.K. Wu, J.Z. Chen, Y.J. Wu, J.Y. Wang, M.N. Yu, F.R. Chen, J.J. Kai, Philos. Mag. A **81**, 1939 (2001)
46 D. Wan, K. Komvopoulos, J. Mater. Res. **20**, 1606 (2005)
47 A. Steegen, K. Maex, Mater. Sci. Eng. R **38**, 1 (2002)
48 C.J. Tsai, K.H. Yu, Thin Solid Films **350**, 91 (1999)
49 D.S. Grummon, J. Zhang, Phys. Stat. Solidi A **186**, 17 (2001)
50 J.-M. Zhang, F. Ma, K.-W. Xu, Surf. Interf. Anal. **35**, 662 (2003)
51 A. Ishida, K. Ogawa, M. Sato, S. Miyazaki, Metall. Mater. Trans. A **28**, A1985 (1997)
52 U. Falke, F. Fenske, S. Schulze, M. Hietschold, Phys. Stat. Solidi A **162**, 615 (1997)
53 E. Horache, J. Van Der Spiegel, J.E. Fischer, Thin Solid Films **177**, 263 (1989)
54 T.-H. Nam, J.-H. Kim, M.-S. Choi, H.-W. Lee, Y.-W. Kim, J. Phys. IV **112**, 893 (2003)
55 A.D. Johnson, M. Fanucchi, V. Gupta, V. Martynov, V. Galhotra, K. Clements, "TiNi as a nano-actuator, experimental verification of excitation by electron-beam heating" (2003); http://www.innovation-on-demand.com/Papers/Nanoactuation_Paper.htm
56 Q. Su, S.Z. Hua, M. Wuttig, J. Alloys Compd. **211**/**212**, 460 (1994)
57 Y.Q. Fu, S. Zhang, M.J. Wu, W.M. Huang, H.J. Du, J.K. Luo, A.J. Flewitt, W.I. Milne, Thin Solid Films **515**, 80 (2006)